

INCREASED SYSTEM PERFORMANCE IN MOBILE ELECTRONICS USING INSULATION-GRAPHITE COMPOSITES

Mitchell Warren¹, Julian Norley², John Allen¹, Jonathan Taylor², Lindsey Keen¹

1. W. L. Gore & Associates, 201 Airport Rd,
Elkton MD, 21921 USA
mwarren@wlgore.com, jallen@wlgore.com, lkeen@wlgore.com

2. NeoGraf Solutions, LLC 11709 Madison Ave.,
Lakewood, Ohio 44133 USA
jnorley@neograf.com, jtaylor@neograf.com

Abstract

Graphite foils with ultra-high spreading capacity and insulation sheets with ultra-low thermal conductivity were combined in a thermally stressed Google Pixel 3XL to reduce steady-state surface touch (skin) temperatures (T_s) by up to 3.2 °C with < 1 °C increase in max junction temperature (T_j) as compared to single-component thermal solutions of graphite, insulation, and air. An axisymmetric conduction model was simulated in COMSOL to determine trends in surface temperature reductions of five unique thermal solutions of comparable thickness (~350 μm). Four of these solutions were fabricated, tested and validated experimentally in Google Pixel 3XL thermal stress testing. The composite yielding the greatest T_s reduction was utilized to demonstrate an increase in steady-state system performance while maintaining a

surface temperature suitable for user safety. The steady-state *3DMark – Sling Shot Extreme* benchmark score increased from 3401 to 3823 resulting in a 12.4% increase in steady-state system performance. The enhanced device performance was linked with material properties by means of steady-state heat flow and thickness testing for through-plane thermal conductivity of insulation, and thermal diffusivity testing for in-plane thermal conductivity of graphite. In-plane conductivity of graphite was validated experimentally in a steady-state heat spreading test where 100 μm foils of high-performance graphite measured ~30% higher spreading capacity than 100 μm foils of synthetic and natural graphite.

Keywords

Graphite, ultra-high spreading capacity, insulation, ultra-low thermal conductivity, composite, heat spreader, thermal conductivity, thickness, surface touch (skin) temperature, hot spot, junction temperature, ambient temperature, steady-state, Google Pixel 3XL (Pixel), system on chip (SoC), 3DMark – Sling Shot Extreme, benchmark score, system performance, user safety.

Nomenclature

k	thermal conductivity (W/m·K)
t	thickness (mm, μm)
T_s	surface touch (skin) temperature (K, °C)
T_j	device junction temperature (K, °C)
ΔT	change in temperature (K, °C)
q''	heat flux (W/m ²)
R''	thermal resistance (K·m ² /W)
t·ΔT	intrinsic heat spreading capacity (μm·K)

Introduction

Thermal spreaders (graphite) and insulators (air, polymers) have been widely and commonly used to address heat challenges in the mobile electronics industry. As the trends for higher power processing and thinner form devices become standard requirements, mobile electronics continue to face a more pressing issue of user safety by means of the surface touch (skin) temperature (T_s).

The Underwriters Laboratories (UL) guidance for T_s is based on direct skin contact for specific temperatures and durations,¹ and is accepted across the mobile electronics industry. Where passive thermal solutions have previously been able to reduce the T_s below specification, many of the commonplace materials such as air and synthetic graphite are facing technical limitations.² In the absence of a thermal solution that maintains system performance, one widely practiced solution is power throttling of the processor, which may reduce system power by up to 50%.³

In thin mobile electronics with relatively low temperatures (< 100 °C) and no active cooling, conduction is the primary mode of heat transfer inside the device⁴; internal convection and radiation are considered negligible in comparison and not discussed further in this work.

Fourier's Law of One-Dimensional Conduction Heat

Transfer, shown in Equation (1), states that the theoretical change in temperature (ΔT) is directly proportional to the thermal resistance (R'') of the heat transfer medium.

$$(1) \quad q'' = \frac{\Delta T}{R''} \left(\frac{W}{m^2} \right)$$

Assuming heat flux (q'') in a given system is constant, ΔT is driven by R'', which is defined as the ratio of thickness (t) to conductivity (k).

$$(2) \quad R'' = \frac{t}{k} \left(\frac{K \cdot m^2}{W} \right)$$

Combining and rearranging Equations (1) and (2), T_s can be viewed as a function of the junction temperature (T_j), t, k, and q'', which is shown in Equation (3) and the accompanying one-dimensional resistance network (Figure 1). In a constrained system with constant q'' and t, T_s can be reduced by lowering k.

$$(3) \quad T_s = T_j - \frac{q'' \cdot t}{k} \quad (K, ^\circ C)$$

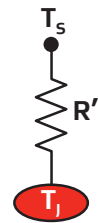


Figure 1: 1D thermal resistance network. Heat flows from T_j to T_s through R''

When a system is expanded into three dimensions of heat transfer (Figure 2), planar heat spreading can be an integral contributor to the resulting T_s. Both in-plane and through-plane conductivities deliver significant contributions to the resultant spreading of heat in a material of given thickness and area. Combining ultra-low (through-plane) conductivity insulation with ultra-high spreading capacity graphite yields a thermal composite solution with exceptional heat spreading performance compared to existing materials used for thermal management in thin mobile electronics.

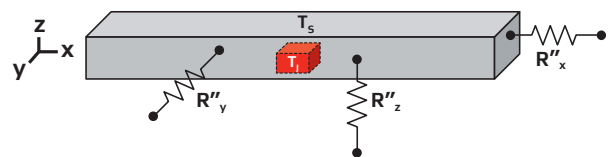


Figure 2: 3D thermal resistance network. Heat moves from T_j (center of device) in multiple directions including toward the surface of interest, T_s.

Material Selection

GORE® Thermal Insulation (W. L. Gore & Associates, Inc.) is an insulating material (“the insulation”) exhibiting ultra-low thermal conductivity, below that of air, in thin sheet form (100 μm and 250 μm). NeoNxGen™ Thermal Management Solutions (NeoGraf Solutions, LLC) includes a thick foil graphite (70 μm to 270 μm) displaying ultra-high intrinsic heat spreading capacity (“high-performance thick graphite”).

Individual layers of insulation and graphite may separately provide a reduction in T_s when placed between a heat source and the surface of interest. Insulation alone is an optimal solution when the ratio of available area to area of the surface hot spot is approximately one-to-one. While insulation is relatively isotropic, graphite exhibits highly anisotropic behavior, favoring thermal conduction in the plane of the material. This utility becomes impactful for T_s reduction when the ratio of available area to area of the surface hot spot approaches two-to-one or greater; in these system architectures, insulation can be combined with graphite to enhance its effective heat spreading capacity. A schematic of the ratio of available area to area of the surface hot spot is illustrated in Figure 3.

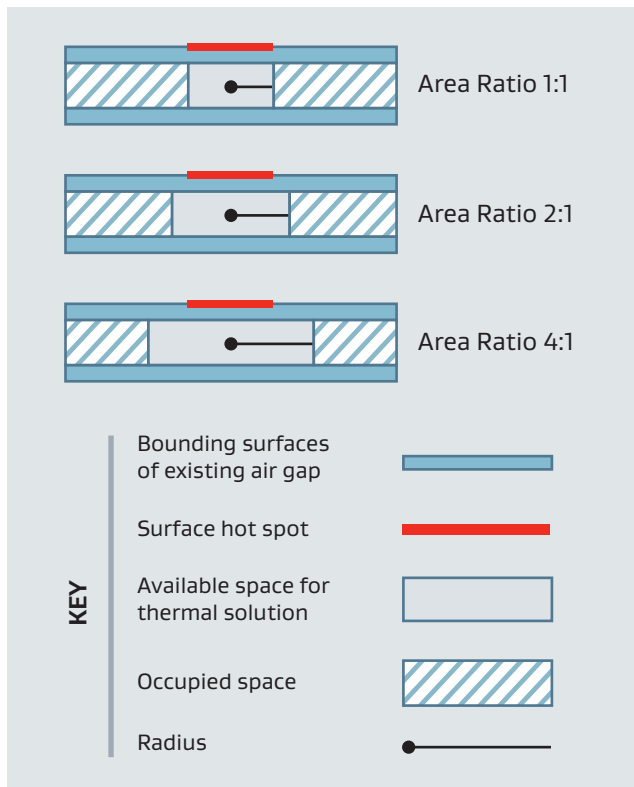


Figure 3: Schematic showing a cross section view of the ratio of available area to area of the surface hot spot. Area is proportional to radius squared.

Insulation Thermal Conductivity Characterization

The insulation is characterized by its distinctively low thermal conductivity, < 0.020 W/m·K, due to a conduction heat transfer phenomenon known as the Knudsen Effect. The Knudsen Effect explains that when the pore diameter in a medium is smaller than the mean free path of air (approximately 70 nm), the path of heat transfer through this medium is disrupted, relative to the path of heat transfer through air in free space.⁵ This principle is often applied through the use of aerogels due to their morphology of high porosity with small pore diameters. The uniqueness of this insulation appears in the form of a homogeneous aerogel structure with ultra-low (and consistent) thermal conductivity and precise thickness resulting in a reliably high thermal resistance. Comparatively, the thermal conductivity of free air at room temperature is 0.026 W/m·K and it increases non-linearly with temperature (0.028 W/m·K at 50 °C),⁶ which can result in variable and insufficient thermal resistance at elevated temperatures ($> 50^\circ\text{C}$) in mobile electronics.

The through-plane thermal conductivity of this insulation is determined by measuring thermal resistance using a heat flow method and material thickness using a precision thickness method. Both tests are conducted with a pressure set point of 6 psi. A heat flow meter (TA Instruments, Model FOX 50), modified from ASTM C518-17, is used to measure thermal resistance under steady-state thermal transmission.⁷ A thin and thick (layered) sample are both tested for thermal resistance. Thickness is then tested for each sample (Instron, Model 5565) using a modified ASTM F36-15 method.⁸ A two thickness resistance procedure is used to calculate through-plane thermal conductivity, shown in Equation (4); this method is used to eliminate any effects of contact resistance in the heat flow method.⁹

$$(4) \quad k = \frac{t_2 - t_1}{R''_2 - R''_1} \left(\frac{W}{m \cdot K} \right)$$

Graphite Thermal Conductivity Characterization

Graphite is used for spreading heat due to its inherently high conductivity in the planar direction and relatively low conductivity in the through-plane direction. Synthetic graphite thickness ranges from less than 25 μm (~1500 W/m·K) up to 100 μm (~600 W/m·K), with in-plane thermal conductivity trending inversely to thickness. Layering thin sheets of high conductivity graphite is a potential way to improve heat spreading capacity at higher thicknesses, though this often leads

to inconsistencies in thermal performance as well as challenges in manufacturing. High-performance thick graphite foils prove to have the thermal conductivity benefits of thin synthetic graphite, up to 1100 W/m·K in-plane, at single-layer thicknesses similar to that of natural graphite. The through-plane conductivity is comparably ~3.5 W/m·K for each grade of graphite.

Two instruments were qualified to test the thermal diffusivity of high-performance thick graphite foils. The first, Angstrom instrument, was developed by Wagoner et al. to measure graphite fibers and named after the inventor of the technique.¹⁰ In this instrument, the temperature of a long, thin specimen is varied sinusoidally at one end and measurements are taken of the resulting heat wave as it propagates along the specimen in a vacuum environment. One end of the specimen is affixed to a heat source while the other end is maintained under light spring tension. Two thermocouples contact the specimen along its length and measure the amplitude and time delay of the temperature wave as it propagates. The amplitude, time delay, and spacing of the thermocouple are used to calculate the thermal diffusivity of the specimen. A second instrument, the TA-33 Thermowave Analyzer, manufactured by Bethel Co., Ltd. irradiates the top surface of a square specimen with a modulated laser beam heat pulse and detects the changes in amplitude and phase of the heat pulse using an infrared detector at the center of the bottom side of the specimen. The laser frequency as well as the horizontal distance between the laser beam and the infrared detector can be varied. The frequency of the laser beam, the change in signal amplitude, and change in phase can be used to calculate thermal diffusivity. In-plane thermal conductivity can then be calculated from thermal diffusivity (α), density (ρ), and specific heat capacity (c_p), shown in Equation (5).

$$(5) \quad k = \alpha \cdot \rho \cdot c_p \left(\frac{W}{m \cdot K} \right)$$

It has been demonstrated that the Angstrom instrument can reliably measure thermal diffusivity on the widest range of graphite specimen thickness, at least 32 μm to 940 μm thick.¹¹ However, the Bethel TA-33 instrument demonstrated similar results and less variation than the Angstrom instrument in the thickness range of 32 μm to 168 μm . Given the smaller specimen size, the non-contact measurement technique, and shorter test cycle time for the Bethel TA-33, it is the preferred thermal diffusivity test

instrument for graphite specimen thicknesses up to 168 μm thick. The Bethel TA-33 test results were used to calculate the thermal conductivity of the 100 μm high-performance thick graphite samples in this paper.

Experimental Tests and Simulation

A series of experiments were conducted to measure the intrinsic heat spreading capacity of graphite, along with steady-state surface temperatures and performance responses for insulation-graphite composites in mobile electronics. Testing results were benchmarked against air and single-component solutions where applicable.

Steady-State Heat Spreading Test

The Steady-State Heat Spreading Test consists of 3-in. x 1-in. graphite strips, heated from one end with an electrical resistance heater applying constant power (4.16 W). Both ends of graphite were fixed in place and solidly in contact with thermocouples via thermal interface materials (TIMs). The temperature drop along the strip was measured at steady-state. A schematic of the test setup is shown in Figure 4.

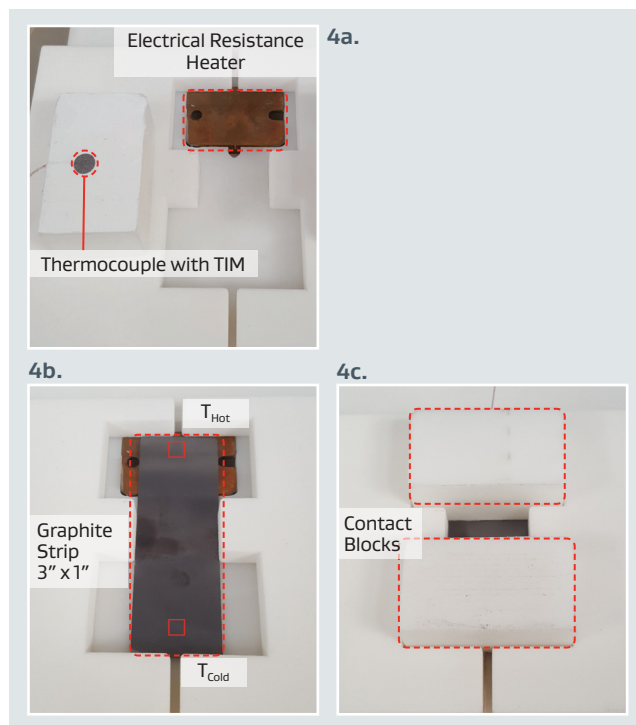


Figure 4 (a, b, c): 4a (top) shows the empty test setup with electrical resistance heater and one contact block with thermocouple-embedded TIM. 4b (lower left) shows the graphite strip placed in the test setup, designating the hot and cold thermocouple locations. 4c (lower right) shows both contact blocks in place, creating solid contact between the thermocouple TIMs and graphite strip.

Test results were analyzed, using Equation (6) to compare intrinsic heat spreading capacity of graphite samples. Temperature drop is multiplied by thickness of individual strips (as measured by compression test with Instron, Model 5565) to account for variations in thickness.

$$(6) \quad t \cdot \Delta T = t \cdot (T_{Hot} - T_{Cold}) \quad (\mu m \cdot K)$$

A lower temperature drop implies greater heat spreading, as the graphite surface temperature is more uniform from end to end. For a material that does not spread heat, the T_{Cold} thermocouple would approximately equal the ambient temperature, resulting in a high value for $t \cdot \Delta T$.

Simulation – Thermal Conduction Model

An axisymmetric thermal conduction model was created in COMSOL to simulate the impact on steady-state T_s and T_j for various thermal solutions in a representative smartphone architecture. The model consists of a constant power heat source, individual material layers, and a device cover; heat transfer coefficients and emissivities can be applied to external surfaces of the heat source and all individual layers. In-plane and through-plane thermal conductivities are defined for all layers and constant across temperatures. The system geometry is defined by a radius and thickness for heat source, material layers, and device cover. Critical model outputs are T_s , displayed in a radial profile along the cover, and maximum T_j on the heat source. Figure 5 shows a schematic of the general model setup and outputs.

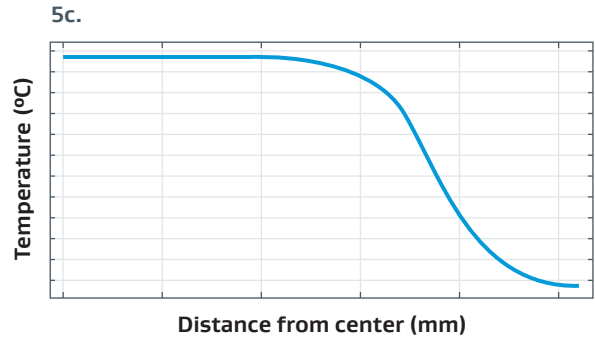
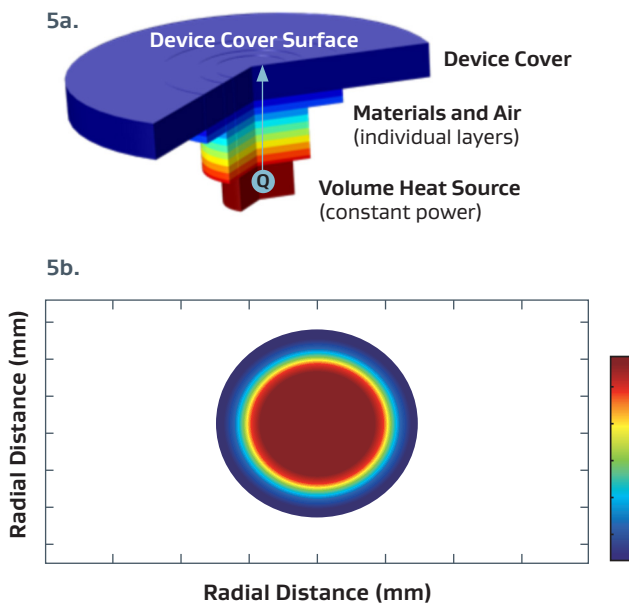


Figure 5 (a, b, c): 5a (top) shows a schematic of the axisymmetric thermal conduction model setup in COMSOL with critical components labeled including volume heat source, material and air layers, and device cover. 5b (middle) and 5c (bottom) show the simulation output in a heat map and radial temperature profile on the device cover surface, respectively.

This simulation focuses on a representative geometry of the Google Pixel 3XL back cover located over the system on chip (SoC); a cross section is shown in Figure 6. Measured thermal conductivity values were applied for insulation (through-plane) and high-performance thick graphite. Literature and data sheets were used to approximate thermal conductivity values for air and glass. Thermal conductivity values used are shown in Table 1. The total thermal gap was fixed at 500 μm for all configurations tested; air was used to fill the remainder of total thickness not filled by materials. All material solutions were modeled at 350 μm thickness to be consistent with physical testing materials. Simulation configurations are detailed in Table 2.

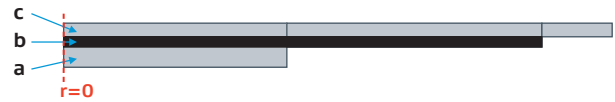


Figure 6: 2D schematic of the axisymmetric thermal conduction model before it is revolved around the “ $r=0$ ” axis. Block “a” represents the heat source with 11.3 mm radius and 1 mm thickness. Block “b” represents an available thermal gap with 24.1 mm radius and 0.5 mm total thickness. Block “c” represents a glass cover with 27.6 mm radius and 0.65 mm thickness.

Table 1: In-plane and through-plane thermal conductivities values used in simulation

Material	In-plane Conductivity (W/m·K)	Through-plane Conductivity (W/m·K)
Air	0.028	0.028
Glass	15	15
High-performance thick graphite	1000	3.5
Insulation	0.018	0.018

Table 2: Configurations simulated in available thermal gap (Block “b”) from Heat Source to Device Cover

Configuration	Material Thickness (mm)	Configuration Depiction
S1 (control)	Air, 0.500	
S2	Insulation, 0.350 Air, 0.150	
S3	Graphite, 0.350 Air, 0.150	
S4	Insulation, 0.175 Graphite, 0.175 Air, 0.150	
S5	Graphite, 0.175 Insulation, 0.175 Air, 0.150	
S6	Graphite, 0.117 Insulation, 0.116 Graphite, 0.117 Air, 0.150	

KEY				
Cover	Heat Source	Air	Insulation	Graphite

Google Pixel 3XL 3DMark Stress Test

An off-the-shelf Google Pixel 3XL (“Pixel”) was purchased and modified to allow for constant power stressing without thermal throttling. UL’s 3DMark – Sling Shot Extreme was chosen for testing as it is a widely-accepted benchmark used to score the physics (CPU) and graphics (GPU) of high-end smartphones.¹² In order to achieve steady-state test results, the Professional Version of 3DMark was purchased and installed on the Pixel to enable infinite looping of the 90-second Sling Shot Extreme benchmark test. All testing was conducted in a still air environment with tightly controlled ambient temperature and humidity. Parameters available for measuring include: surface point temperatures via thermocouples, images via IR camera (Fluke, Model Ti55), internal component temperatures (CPU, GPU, etc.) via built-in thermistors, CPU and GPU clock frequencies, and system

performance via Sling Shot Extreme benchmark score. An initial stress test was run in the out-of-box condition with IR imaging (Figure 7). Hot spot locations were identified and chosen for placement of thermocouples via TIMs (Figure 8).

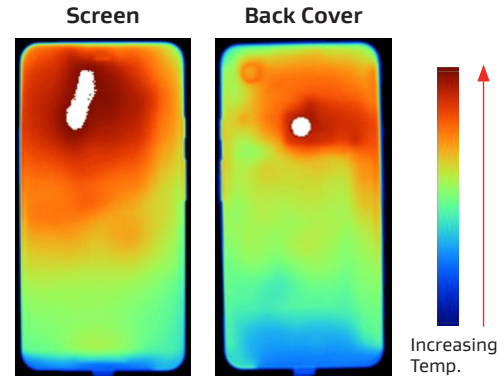


Figure 7: IR images of screen (left) and back cover (right) on the Google Pixel 3XL. A numberless temperature scale is shown to indicate directional trends between color and temperature. Surface hot spots are represented by the white areas.

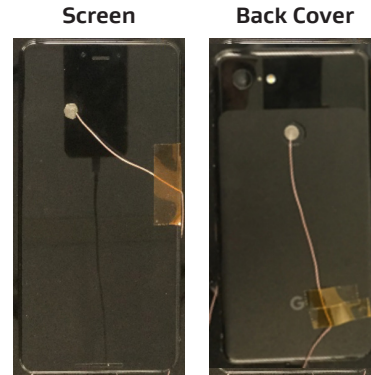


Figure 8: Screen (left) and back cover (right) with thermocouples attached via TIMs on the Google Pixel 3XL. Thermocouples were placed precisely to measure temperatures at the surface hot spot locations.

The Pixel back cover was removed by means of heating and breaking adhesive. A conformable polymer was placed inside the back cover at seven different locations near the SoC (Figure 9) to determine the space available for a thermal solution; the back cover was then replaced to compress the polymer into the existing air gap at each location. The back cover was removed again and thickness at all locations was measured via snap gauge on the compressed polymer. This process was repeated twice more and all thickness measurements per location averaged. Thickness means are detailed in Table 3.



Figure 9: Google Pixel 3XL with back cover removed. Existing air gap thickness measured by conformable polymer at seven locations shown.

Table 3: Air gap measurements near SoC in closed Pixel device

Location	Mean Gap Measurement (mm)
1	0.900
2	0.625
3	0.520
4	0.520
5	0.440
6	0.450
7	0.640

In order to avoid mechanical compression in Locations 5 and 6, a nominal thickness of 350 μm was chosen for all thermal solutions. Physical materials for testing include 110 μm insulation sheets, 110 μm graphite foils and 5 μm acrylic double-sided tape. Materials and example configurations are illustrated in Figure 10.

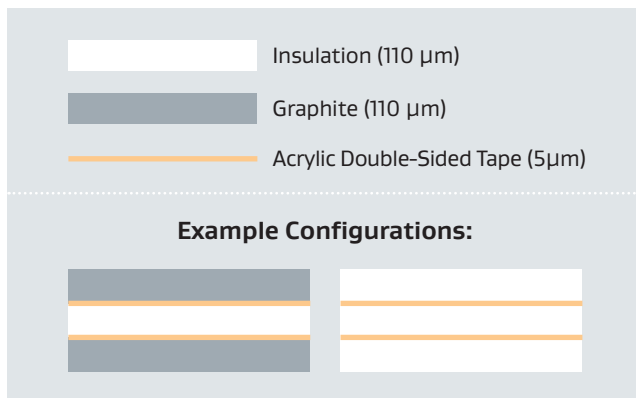


Figure 10: Depiction of physical materials for testing and example configurations of materials layered with adhesive.

The part geometry, shown in Figure 11, was chosen to maximize area with no or minimal disruption to internal components. For simplicity, only configurations with uniform thickness and layers with identical shape and area were considered. Further optimization in layer thicknesses and sizes are possible to achieve form, fit, or functional goals. A cross section schematic through the thickness of the phone is depicted in Figure 12. Simulation results were analyzed to inform material configurations chosen for Pixel testing.

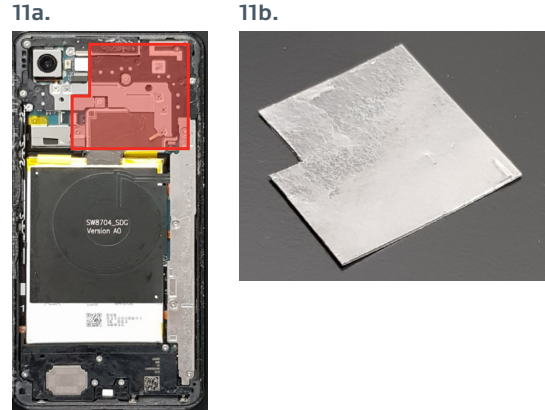


Figure 11 (a, b): 11a (left) shows placement of the part inside the back cover. 11b (right) shows a composite sample cut to fit the designated geometry. Part area measured to be 1825 mm^2 .

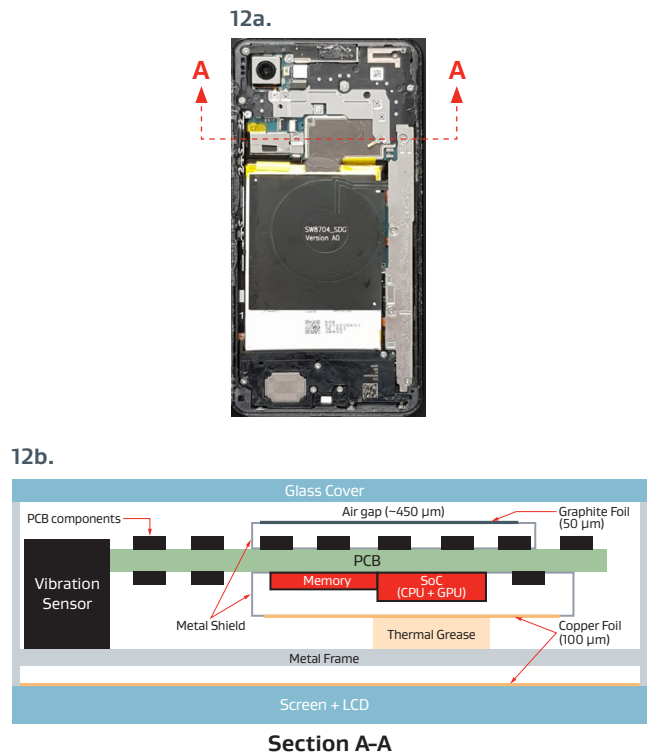


Figure 12 (a, b): 12a (top) denotes the location of cross section A-A in the Pixel. 12b (bottom) shows a schematic of section A-A through the thickness of the device.

Results

Steady-State Heat Spreading Test

Synthetic, natural and high-performance graphite grades were tested, all at 100 μm nominal thickness; $t \cdot \Delta T$ values were obtained using Equation (6). Six individual samples of each graphite were tested in a randomized experiment. Results are shown in Figure 13.

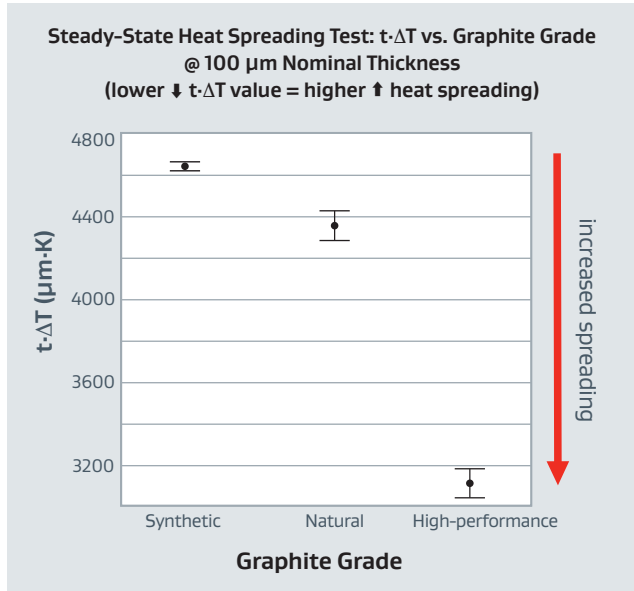


Figure 13: Graph (means and standard deviations) of Steady-State Heat Spreading Test $t \cdot \Delta T$, $n=6$ per graphite grade.

High-performance thick graphite exhibited the lowest $t \cdot \Delta T$ value with a mean of $\sim 3100 \mu\text{m} \cdot \text{K}$. This value is 29% lower than the mean $t \cdot \Delta T$ value for natural graphite ($\sim 4350 \mu\text{m} \cdot \text{K}$), and 33% lower than the mean $t \cdot \Delta T$ value for synthetic graphite ($\sim 4650 \mu\text{m} \cdot \text{K}$).

Simulation – Thermal Conduction Model

Power and heat transfer coefficients were iterated to achieve cover and heat source temperatures relevant to Pixel device testing. Surface emissivity was neglected for this simulation. Parameters chosen for all test configurations are shown in Table 4.

Table 4: Simulation inputs for all test configurations

	Power (W)	Device Cover Heat Transfer Coefficient ($\text{W}/\text{m}^2 \cdot \text{K}$)	Heat Source Heat Transfer Coefficient ($\text{W}/\text{m}^2 \cdot \text{K}$)	Material Layers Heat Transfer Coefficient ($\text{W}/\text{m}^2 \cdot \text{K}$)
Set Point Value	1.5	20	25	1

Configurations S1 through S6 were simulated and outputs displayed in Figure 14 with results detailed in Table 5. All configurations are compared to the control scenario, Configuration S1 (air only). A zoomed in graph of cover surface temperature for graphite and insulation-graphite composite configurations (S3, S4, S5 and S6) is displayed in Figure 15.

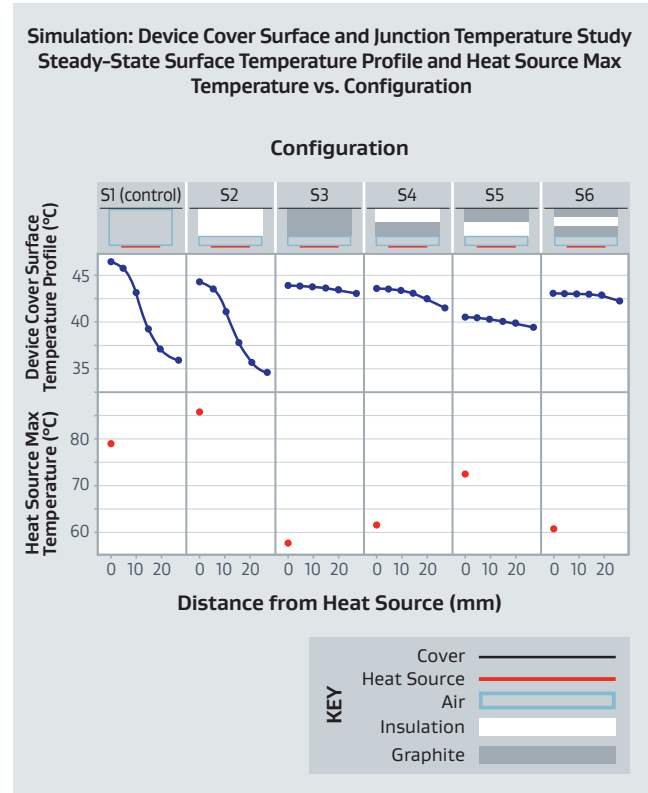


Figure 14: Simulation results by configuration. The top graph displays a radial temperature profile along the device cover surface from device center ($r = 0 \text{ mm}$) to device edge ($r = 27.6 \text{ mm}$). The bottom graph displays a single value for the device heat source max temperature.

Table 5: Simulation results for max temperatures on cover surface and heat source

Configuration	Cover Surface Max Temperature ($^{\circ}\text{C}$)	Heat Source Max Temperature ($^{\circ}\text{C}$)
S1 (control)	46.55	78.82
S2	44.28	85.43
S3	43.79	57.58
S4	43.54	61.73
S5	40.52	72.48
S6	42.96	60.42

Simulation: Device Cover Surface and Junction Temperature Study for Configurations including Graphite
Steady-State Surface Temperature Profile vs. Configuration

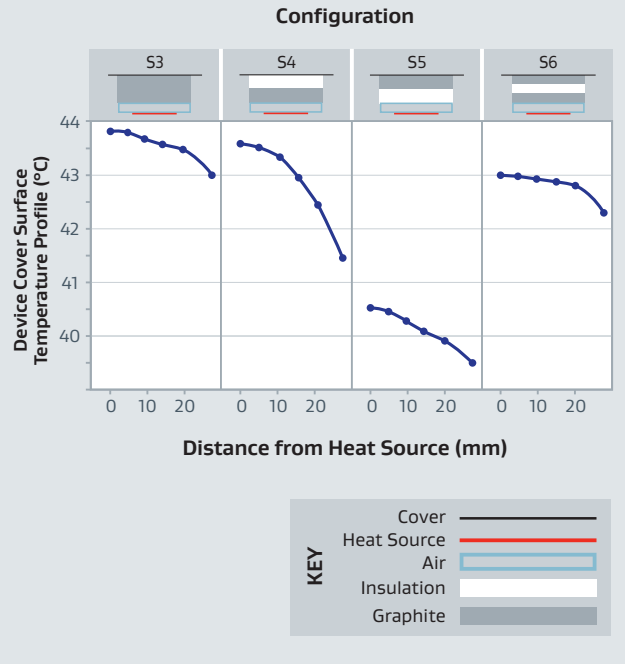


Figure 15: Zoomed into top graph of Figure 14 for the graphite only and insulation-graphite composite configurations (S3, S4, S5, and S6).

Configuration S5 yields the greatest reduction of max surface temperature compared to the control (Configuration S1). For all configurations tested, the max temperatures on device cover surface and heat source occur at the device center ($r = 0$). As heat travels radially from the device center, the temperature decreases. When insulation is introduced into the system (Configuration S2), the temperature profile along the surface looks similar to that of the control, though the magnitude is shifted down at each respective location along the surface. This effect is a result of the insulation’s ultra-low conductivity and propensity to redirect heat toward the heat source, causing an increase in Tj. When graphite and insulation-graphite composites are introduced into the system (Configurations S3, S4, S5, and S6) the max surface temperature is reduced while the radial temperature profile is increased relative to the control. This result occurs due to graphite’s preferential planar spreading of heat, producing a more uniform heat distribution along the device surface.¹³ The simulated Tj is maintained or reduced for these four configurations relative to the control.

Google Pixel 3XL 3DMark Stress Test

Back Cover Touch Temperature Study

Configurations S1, S2, S3, S5, and S6 from simulation were selected for Pixel device testing and constructed with physical materials described in Figure 6 above; device test configurations are titled D1, D2, D3, D5, and D6 with D1 as the control scenario. The CPU and GPU frequencies were set at 2169.6 MHz and 675 MHz, respectively. Frequencies were recorded and verified at the end of each test run. Benchmark scores were recorded to show performance consistency across all test runs. Ambient temperatures in the still-air environment were held between 21.6 and 21.8 °C for all testing. All configurations were tested three times to steady-state (> 90 minutes) in a randomized experiment. After each test run, the Pixel was cooled down to idle operating temperature and opened up to setup the next test run. The steady-state back cover hot spot touch temperatures and GPU max temperatures are shown in Figure 16. IR images of the back cover are shown in Figure 17. Depictions, thicknesses, and measured outputs (means and standard deviations) for all tested configurations are detailed in Table 6.

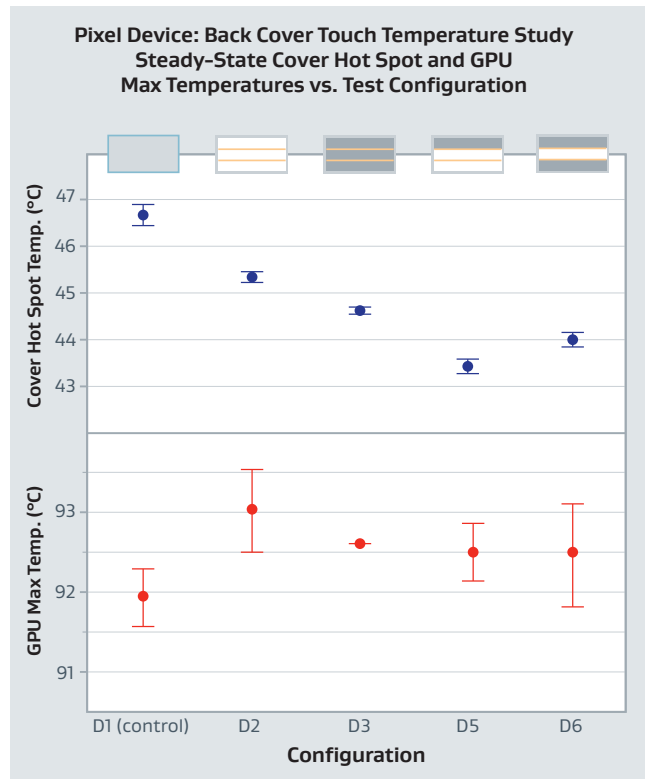


Figure 16: Steady-state graph (means and standard deviations) of back cover hot spot temperature (top) and GPU max temperature (bottom) for all configurations tested in Pixel device, n=3 per configuration.

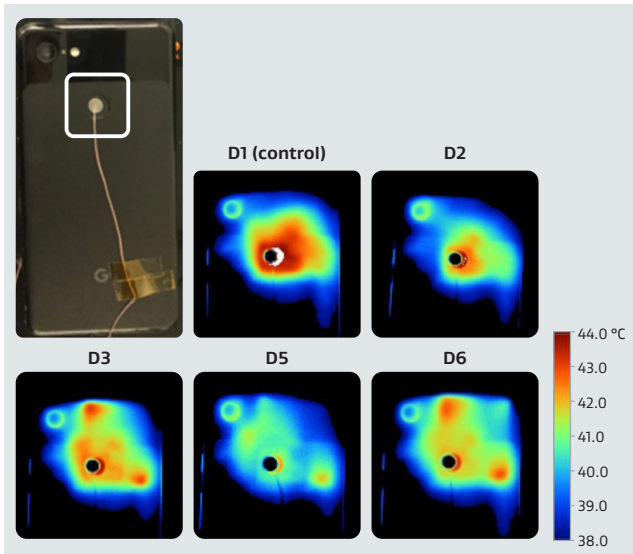


Figure 17: Zoomed in IR images over back cover hot spot for all configurations tested in Pixel device.

Table 6: Pixel Device Results: Back Cover Touch Temperature Study

Configuration	Cover Hot Spot Temp. (°C)		Screen Hot Spot Temp. (°C)		CPU Max Temp. (°C)		GPU Max Temp. (°C)		Sling Shot Extreme Benchmark Score	
	Mean	St. Dev.	Mean	St. Dev.	Mean	St. Dev.	Mean	St. Dev.	Mean	St. Dev.
D1 (control)	46.7	0.21	49.7	0.25	84.8	0.17	91.9	0.35	4374.3	1.15
D2 (344 μm)	45.4	0.12	50.5	0.10	86.1	0.51	93.0	0.51	4377.7	1.15
D3 (339 μm)	44.6	0.06	50.1	0.10	85.4	0.65	92.6	0.00	4375.7	1.53
D5 (347 μm)	43.5	0.15	49.9	0.26	85.6	0.17	92.5	0.35	4372.3	2.08
D6 (347 μm)	44.0	0.15	49.9	0.26	85.6	0.51	92.5	0.67	4375.0	1.00

All test configurations produced unique back cover touch temperatures with high precision, and all were distinctly lower than the control (Configuration D1). In agreement with the simulations, Configuration D5 presented the greatest back cover touch temperature reduction at 3.2 °C below the control. Configurations D6, D3, and D2 reduced the back cover touch temperature by 2.7, 2.1, and 1.3 °C, respectively. Screen temperatures increased from the control by < 1 °C for all configurations tested and < 0.5 °C for composite configurations. CPU and GPU

temperatures increased from the control by < 1.5 °C for all configurations tested and < 1 °C for composite configurations. The Pixel back cover touch temperature study results validate the directional trend of device surface temperature for the emulated configurations in the simulation study. The directional trend of junction temperatures in simulation was not replicated by the relatively consistent CPU and GPU temperatures in physical device testing. This difference is likely attributed to the complexity of thermal architecture near the SoC in the real Pixel device.

System Performance and Safe Touch Temperature Study

A continuation study was created to determine the allowable system performance increase when enabled by insulation-graphite composites; Configuration D5 was selected for this study. Out-of-box throttling conditions were restored to the Pixel and all thermal solutions were removed, leaving air only. The back cover touch temperature was measured during steady-state power throttling and recorded for three test runs. Configuration D5 was installed and frequencies were set to match the steady-state cover temperature from the throttled control runs. The appropriate frequencies for testing were determined to be 1996.8 MHz and 596 MHz for the CPU and GPU, respectively. Frequencies, cover hot spot temperature, benchmark score and Frames per Second were measured and compared between the two test scenarios. A smoothed plot of benchmark score, CPU frequency, and GPU frequency vs. run time for all six test runs is displayed in Figure 18. Mean steady-state cover temperature, benchmark score, and Frames per Second are shown in Figure 19. Details are summarized in Table 7.

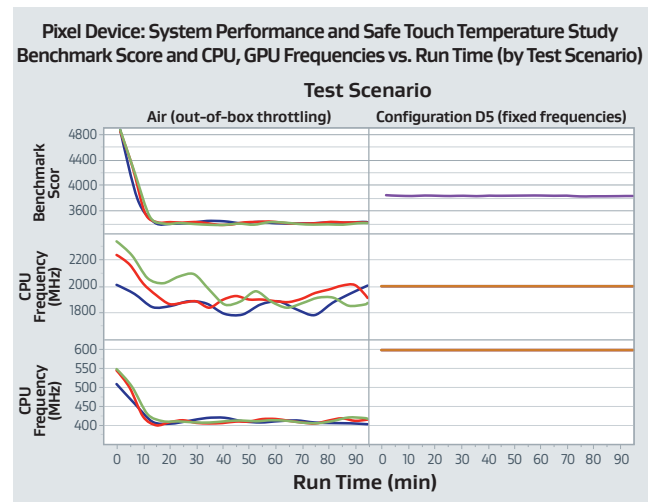


Figure 18: Transient graph (smoothed) of benchmark score (top), CPU frequency (middle), and GPU frequency (bottom) for air only, out-of-box throttling (left) and Configuration D5, fixed frequencies (right) in Pixel device, n = 3 per test.

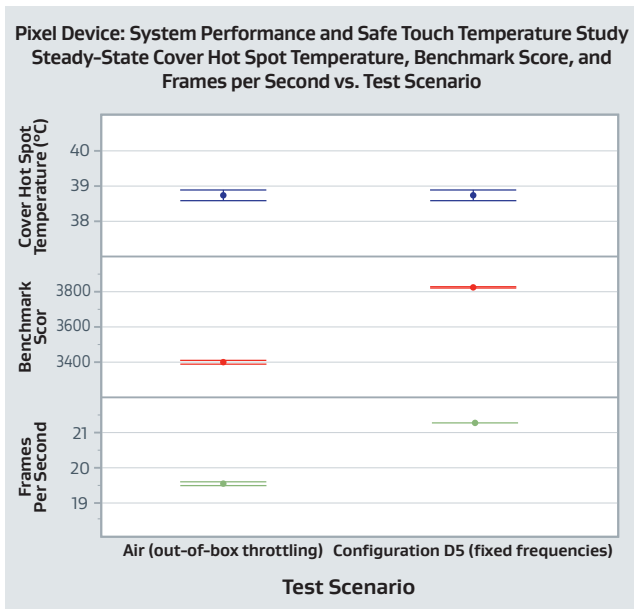


Figure 19: Steady-state graph (means and standard deviations) of back cover hot spot temperature (top), Sling Shot Extreme benchmark score (middle), and Frames per Second (bottom) for air only, out-of-box throttling and Configuration D5, fixed frequencies in Pixel device, n=3 per configuration.

Table 7: Pixel Device Results: System Performance and Safe Touch Temperature Study

Test Scenario	Cover Temp (°C)		Sling Shot Extreme Benchmark Score		Frames per Second	
	Mean	St. Dev.	Mean	St. Dev.	Mean	St. Dev.
Air (out-of-box throttling)	38.7	0.15	3401.0	8.19	19.5	0.06
Configuration D5 (fixed frequencies)	38.7	0.15	3822.7	3.06	21.3	0.00

The mean steady-state cover touch temperature achieved during out-of-box throttling is 38.7 °C in the controlled test environment at 21.7 °C; this temperature is related to UL 62368-1 mobile electronics touch (skin) temperatures at prolonged durations. In this scenario, the mean steady-state benchmark score and Frames per Second are 3401 and 19.5, respectively. When Configuration D5 is placed inside the back cover, the benchmark score is increased to 3823 and Frames per Second increased to 21.3, marking a ~12% increase in system performance, while maintaining the safe surface temperature limit set for the out-of-box throttling condition.

Summary/Conclusion

Graphite foils with ultra-high spreading capacity and insulation sheets with ultra-low thermal conductivity were combined in a modified Google Pixel 3XL to reduce surface touch (skin) temperatures and increase system performance while minimally impacting the device junction temperature. The experimental results for device surface temperature of five unique thermal configurations were used to validate a comparable simulation study using an axisymmetric thermal conduction model. The resulting surface temperature reductions from insulation-graphite composites exceeded those of air, insulation alone, and graphite alone, when filling the same area and thickness. One insulation-graphite composite configuration was further tested in comparison to an out-of-box condition, and was found to improve system performance in a UL benchmark test by ~12% while maintaining the out-of-box cover surface temperature limits.

The results demonstrated by insulation-graphite composites in Pixel device testing and simulation can be explained by the exceptional thermal properties exhibited by these two materials. Through-plane thermal conductivity for the insulation was measured and calculated using a heat flow method on a TA-FOX 50, a thickness method on an Instron-5565, and a two thickness resistance procedure. In-plane thermal conductivity for high-performance thick graphite was measured and calculated using a thermal diffusivity method on a Bethel TA-33. The heat spreading capacity of the 100 μm high-performance thick graphite was compared to 100 μm synthetic and natural graphite and validated experimentally in a steady-state heat spreading test.

High-performance insulation-graphite composites may have vast utility in the high-powered, thin architectures of mobile electronics. It is important to note that each mobile electronic system may exhibit unique thermal challenges given system power, available space, and/or other constraints. For this reason, the optimal design configuration (area, thickness, orientation) should be determined by virtue of device-specific simulation and testing. The case study presented in this paper demonstrates an art of possibility for enhancing thermal management in mobile electronics; two leading-edge materials, when combined, yield a thermal solution with performance greater than the sum of its parts.

References

1. UL, UL. "62368-1: 2017 Audio/video, information and communication technology equipment - Part 1: Safety requirements." (2017).
2. Wagner, Guy, and William Maltz. "Thermal management challenges in the passive cooling of handheld devices." 19th International Workshop on Thermal Investigations of ICs and Systems (THERMINIC). IEEE, 2013.
3. Wagner, Guy R. "A study of the maximum theoretical power dissipation of tablets under natural convection conditions." 20th International Workshop on Thermal Investigations of ICs and Systems. IEEE, 2014.
4. Luo, Zhaoxia, et al. "System thermal analysis for mobile phone." Applied Thermal Engineering 28.14-15 (2008): 1889-1895.
5. Bi, C., G. H. Tang, and W. Q. Tao. "Prediction of the gaseous thermal conductivity in aerogels with non-uniform pore-size distribution." Journal of Non-Crystalline Solids 358.23 (2012): 3124-3128.
6. Kannuluik, W. G., and E. H. Carman. "The temperature dependence of the thermal conductivity of air." Australian Journal of Chemistry 4.3 (1951): 305-314.
7. ASTM C518 – 17 Standard Test Method for Steady-State Thermal Transmission Properties by Means of the Heat Flow Meter Apparatus
8. ASTM F36 – 15 Standard Test Method for Compressibility and Recovery of Gasket Materials
9. LaserComp, Inc.. "Tests of thin samples stacked (using FOX50 instrument)" Application Note AN-TSS © 2008 (October 23).
10. Wagoner, G., Skokova, K.A. and Levan, C.D., "Angstrom's Method for Thermal Property Measurements of Carbon Fibers and Composites", The American Carbon Society, CARBON Conference, 1999.
11. Beyerle, R., Smalc, M., Kantharaj, R., Taylor, J., Norley, J., "Thermal Diffusivity Characterization of Thick Graphite Foils", 35th Semi-Therm Symposium, 2019.
12. 3DMARK® Technical Guide, Underwriters Laboratories, Fremont, CA, 2020.
13. Xiong, Yin, et al. "Thermal tests and analysis of thin graphite heat spreader for hot spot reduction in handheld devices." 2008 11th Intersociety Conference on Thermal and Thermomechanical Phenomena in Electronic Systems. IEEE, 2008.

Contact Us

For additional assistance, please contact a Gore representative.

INTERNATIONAL CONTACTS

Australia	+61 2 9473 6800	Mexico	+52 81 8288 1281
Benelux	+49 89 4612 2211	Scandinavia	+46 31 706 7800
China	+86 21 5172 8299	Singapore	+65 6733 2882
France	+33 1 5695 6565	South America	+55 11 5502 7800
Germany	+49 89 4612 2211	Spain	+34 93 480 6900
India	+91 22 6768 7000	Taiwan	+886 2 2173 7799
Italy	+39 045 6209 240	United Kingdom	+44 1506 460123
Japan	+81 3 6746 2570	USA	+1 410 506 7812
Korea	+82 2 393 3411		

W. L. Gore & Associates

401 Airport Road · Elkton, MD 21921 · USA
· Phone: +1 410 506 7812 (USA) · Toll free: +1 800 523 4673
· Fax: +1 410 506 8749 · Email: thermal@wlgore.com

gore.com/thermal

FOR INDUSTRIAL USE ONLY. Not for use in food, drug, cosmetic or medical device manufacturing, processing or packaging operations. All technical information and advice given here is based on Gore's previous experiences and/or test results. Gore gives this information to the best of its knowledge, but assumes no legal responsibility. Customers are asked to check the suitability and usability in the specific application, since the performance of the product can only be judged when all necessary operating data are available. The above information is subject to change and is not to be used for specification purposes.

Gore's terms and conditions of sale apply to the sale of the products by Gore. GORE and designs are trademarks of W. L. Gore & Associates.

©2020 W. L. Gore & Associates, Inc.

